Robotic Skins with Integrated Actuation, Sensing, and Variable Stiffness

Dylan S. Shah¹, Stephanie J. Woodman¹, Trevor L. Buckner¹, Ellen J. Yang¹, and Rebecca K. Kramer-Bottiglio^{1*}

Abstract—Soft robots are often designed to accomplish a single function and cannot be repurposed for other tasks. In an effort to create multi-functional robots, researchers have proposed robotic skins, which are flexible, planar substrates with embedded actuation and sensing that can be applied to different soft bodies. By "roboticizing" otherwise inert bodies from their surface, robotic skins can be repurposed to create bespoke soft robots as needed. However, current robotic skins are unable to support their own structure and can only attain a single function in the absence of a host. Here, we present a variable stiffness robotic skin (VSRS), a concept that integrates stiffness-changing capabilities, sensing, and actuation into a single, thin modular robot design. Reconfiguring, reconnecting, and reshaping VSRSs allows them to achieve new functions both on and in the absence of a host body. We demonstrate how a single set of skins with PneuFlex-style pneumatic actuators, a geometricallypatterned polyethylene terepthalate (PET) jamming membrane, and liquid metal-based capacitive sensors can operate as closedloop locomotion robots while being able to support weight during locomotion, as well as stiffen to hold complex shapes. To highlight the generality of the concept and illuminate the design space, we also test a second embodiment with McKibben actuators and a woven-mesh jamming membrane that can be reconfigured to serve in a manipulation context. We see VSRSs having application as adaptable linkages in larger robots, smart reconfigurable garments, and reconfigurable active structures, thereby allowing the robotic system to adapt to time-varying task requirements.

Index Terms—Soft Robot Materials and Design, Cellular and Modular Robots, Biologically-Inspired Robots

I. INTRODUCTION

OST robots can execute a fixed range of rigid-body motions and are unable to adapt to unexpected changes in performance needs, limiting their use to a finite number of applications or environments. In contrast, many biological systems thrive across a wide range of tasks and environments, leveraging incredible cognitive plasticity [1], and an ability to adapt in stiffness to perform both forceful and gentle tasks [2]. By taking cues from nature on matters of mind and body, biologically inspired soft robots leverage new approaches to functioning in unpredictable environments [3]. Foundational

Manuscript received: July 11, 2023; Revised October 18, 2023; Accepted November 12, 2023. This paper was recommended for publication by Editor Xinyu Liu upon evaluation of the Associate Editor and Reviewers' comments. This work was supported by a National Science Foundation (NSF) EFRI Grant (EFMA-1830870). DSS was supported by a NASA Space Technology Research Fellowship (grant 80NSSC17K0164). SJW was supported by a NASA NSTGRO Fellowship (80NSSC22K1188).

¹D. S. Shah, S. J. Woodman, T. L. Buckner, E. J. Yang, and R. K. Kramer-Bottiglio are with the Department of Mechanical Engineering & Materials Science, School of Engineering and Applied Science, Yale University, New Haven, CT 06520, USA. (dylan.shah.50@aya.yale.edu, stephanie.woodman@yale.edu, ellen.yang@yale.edu, rebecca.kramer@yale.edu)

Digital Object Identifier (DOI): see top of this page.

studies on automated gait adaptation [4], adaptive morphogenesis [5], and variable stiffness materials [6] are beginning to yield synthetic systems with life-like adaptive capabilities.

With an eye toward the design of specifically multi-purpose soft robots, one common approach is the use of modular, reconfigurable robots [7]. For example, Robertson *et al.* proposed soft cylindrical modules that can be reconfigured between locomotion and manipulation tasks [8]. More recently, Li *et al.* proposed meter-scale modular soft robots for locomotion and manipulation [9]. Our own prior work includes modular soft robotic skins: two-dimensional (2D) elastic membranes with embedded actuators and sensors, which, when attached to the surface of a host three-dimensional (3D) soft object, can impart controlled motion onto that object and "roboticize" it [10]. Robotic skins have previously been applied, removed, and re-applied to different host objects to achieve multiple tasks including locomotion, manipulation, grasping, wearability, and shape-change [10], [11], [12].

However, soft modular robots bring challenges common to all soft robots, including reduced payload capacity. To allow soft robotic modules to gain some of the advantages of rigid materials, numerous variable-stiffness materials have been proposed (as reviewed by Manti *et al.* [6]), including stimuli-responsive materials [13] and antagonistic actuators [14]. Variable-stiffness in thin systems has been achieved by applying a vacuum to thin membranes filled with layers of inextensible material to achieve "layer jamming" [15], [16]. To apply layer jamming to modular robotic skins and allow them to lock into general biaxially-curved shapes, the skins need to stretch while unjammed [17]. Recent studies have begun to investigate stretchable variable stiffness solutions, including jamming skins made by cutting intricate patterns in polyethylene terephthalate (PET) [18], and jamming meshes [19].

Here, we build upon this body of work by introducing the concept of a variable stiffness robotic skin (VSRS), a soft robot module that integrates actuation, sensing, and variable stiffness. VSRSs retain the benefits of prior robotic skins and introduce adaptive stiffness to achieve additional functions such as shape-locking and load-bearing (Fig. 1). Through two embodiments that illuminate the trade-offs of this design space, we demonstrate how modular VSRSs can be used in different configurations to locomote while carrying a payload and form a continuum manipulator with a tunable workspace.

II. VSRS OVERVIEW

A VSRS has three primary functional components: a variable stiffness mechanism [6], actuators [20], and sensors [21]. Additionally, an inert substrate provides spatial organization

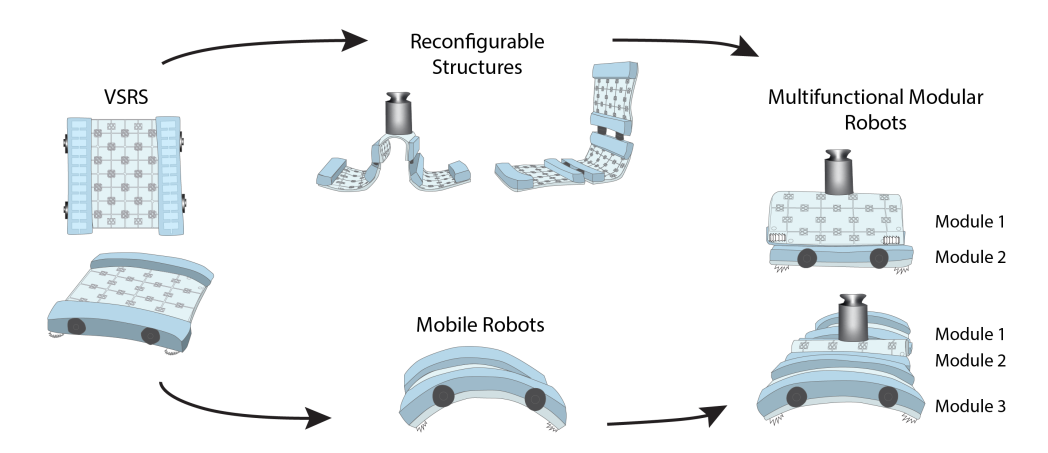


Fig. 1. A variable stiffness robotic skin (VSRS) is a reconfigurable, modular sheet containing sensors, actuators, and variable stiffness components. After use in one task, each VSRS may be reconfigured into a different shape and (un)joined with other VSRSs for use in a different task, such as locomotion and manipulation. Multiple embodiments of VSRSs are possible. Here, we show a design with pneumatic actuators, capacitive stretch sensors, and a stretchable vacuum jamming variable-stiffness core.

and a way to attach to other skins. Important performance trade-offs to consider when selecting components include thickness, weight, the stiffness-switching ratio of the variable stiffness materials, actuator performance, and sensor resolution. In this work, we sought to achieve sensors with long-term stability and low noise, actuators with a high strength-to-weight ratio, and fast-acting variable stiffness mechanisms to enable real-time shape transitions.

The VSRS concept is independent of specific component choices, which we demonstrate by realizing two VSRS embodiments, each square-shaped with nominal edge length of 13 cm, but varying in their selected components. The first embodiment, "PET VSRS," was made using fiber-reinforced pneumatic actuators (similar to PneuFlex [22]), capacitive stretch sensors (with oxidized liquid metal [23] electrodes), and jammed PET sheets [18] (Fig. 2). The second VSRS embodiment, "mesh VSRS," uses McKibben actuators [24], the same capacitive stretch sensors, and jammed woven mesh sheets [19]. While both embodiments satisfy our definition of VSRS, component choices yield unique advantages and corresponding suitabilities to different use cases. Specifically, we found that the PET VSRS had higher stiffness and payload capacity, but couldn't wrap into a continuum manipulator configuration. However, by integrating actuation, sensing, and variable stiffness capabilities into a single modular design, all VSRSs including those demonstrated can serve as multifunctional, planar soft robots without requiring a host body, in contrast to equivalent single-stiffness skins.

III. PET VSRS RESULTS

A. Manufacturing

We used a layer-by-layer method to manufacture the VSRS while minimizing thickness (Fig. 2). First, silicone (Dragon Skin 10, abbreviated as DS10, Smooth-On, Inc.) was rod-coated to make a thin layer and cured at room temperature. Next, an oxidized liquid metal paste was created by shear-mixing eutectic gallium-indium (EGaIn) with a laboratory stirrer (IKA EuroStar 20 digital) at 400 rpm for 2 hr at 150 °C,

to encourage the formation of solid gallium oxide throughout the liquid EGaIn (inspired by Wang *et al.* [23]). This oxidized gallium-indium (OGaIn) paste was manually spread over a laser-cut paper stencil to make four strips that served as the ground layer of the VSRS stretch sensors. Wires were added at one end of each electrode. We then applied a layer of silicone (EcoFlex 00-30, Smooth-On, Inc.) as a dielectric, let it cure, added another layer of OGaIn electrodes and wires, and added a final layer of EcoFlex 00-30 to encapsulate the sensors.

To integrate layer jamming capabilities, we added pneumatic tubing and 15 layers of stretchable, geometrically-patterned PET sheets (cut from 0.01" PET, McMaster-Carr). Each PET sheet comprised a pattern of inextensible polygons joined by extensible serpentine springs (as in our prior work [18]), thereby granting the aggregated sheets flexibility and elasticity while unjammed, and rigidity when under vacuum. To aid in alignment, each PET sheet had a hole cut into each corner. After stacking the sheets together, the alignment holes were filled with SilPoxy, and small weights were placed on the layers to ensure they stayed close together. Then, we folded and sealed the membrane with DS10. Utilizing additional PET layers would increase the jamming ratio at the cost of raising the unjammed stiffness, and we empirically chose 15 layers to balance these two objectives.

PneuFlex actuators were made by casting and curing DS10 in a 3D-printed mold and subsequently placing the molded part onto a piece of fabric impregnated with uncured DS10. Once the molded part and silicone-fabric cured together, we wrapped the actuator in fiber-reinforced silicone [25] to encourage uniaxial bending, and attached tubing with SilPoxy (Smooth-On, Inc.). Finally, we used SilPoxy to attach velcro, magnetic snaps, and laser-cut acrylic feet.

We controlled the modules using a vacuum pump, pneumatic pressure regulators [26], and an Arduino Uno (Arduino AG). The stretch sensors' capacitances were measured using an MPR121 capacitive sensing integrated circuit (Resurgent Semiconductor) due to its excellent onboard noise rejection features, and sent to a PC for recording.

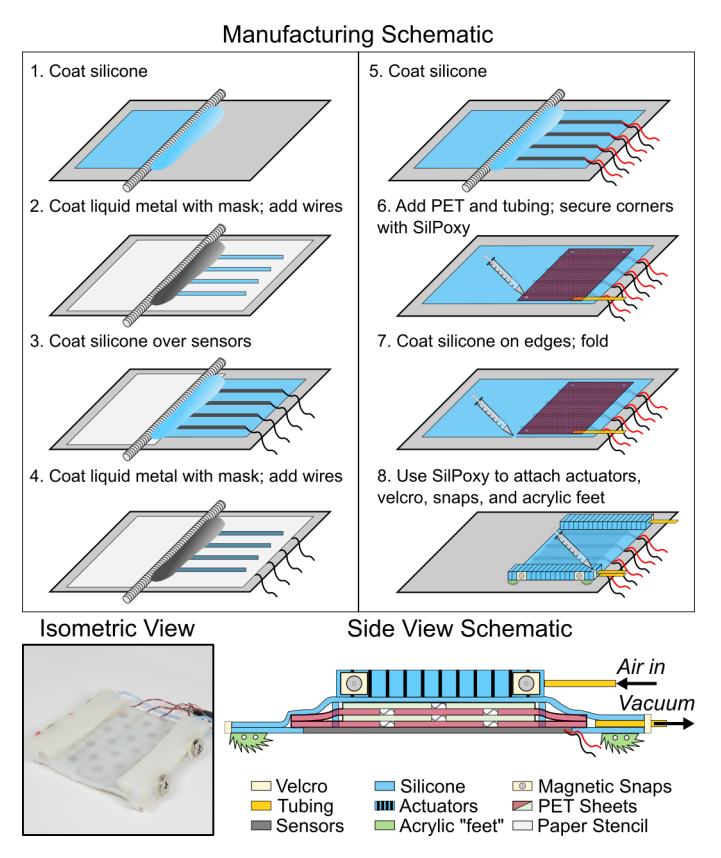


Fig. 2. Design and manufacturing of a PET VSRS. First, the jamming skin membrane was made from successive layers of silicone and oxidized liquid metal paste (steps 1-5). To make the membrane into a robotic skin, we added PET sheets and tubing, sealed the membrane, and attached actuators, low-profile velcro, magnetic snaps, and acrylic feet to the skin (steps 6-8). Below the manufacturing schematic, we have included an isometric-view photograph of the finished 13 cm square skin, a side view schematic, and a legend corresponding to both schematics.

B. Mechanical characterization

To quantify the stiffness-changing capabilities of the PET VSRS, we tested the skins in a flat, three-point bending configuration using a materials testing machine (Instron 3345). Three samples were tested five times each when unjammed at atmospheric pressure and jammed at $-80~\mathrm{kPa}$, with the flexure fixture's test anvil (Instron 2810-400) oriented both perpendicular and parallel to the actuators. This experimental design allowed us to test how stiffness was influenced by both the vacuum pressure as well as the skins' anisotropic properties introduced by the actuators. An upper loading anvil was lowered at 60 mm/min to deflect the skins a total of 30 mm (plotted to 20 mm in Fig. 3A to highlight the transition from linear to nonlinear regions), with the span between the lower anvils set at 80 mm.

The force vs. displacement data resulting from the three-point bending tests suggest a relatively uniform behavior within each sample (visualized as narrow error clouds in Fig. 3A). In the jammed configurations, the skins exhibited a linear regime until the jammed layers slip, after which the slope and linearity both decrease [15]. Observed variations between different samples may be due to the more manual steps in the manufacturing process, such as attaching the actuators.

From the stiffness curves in Fig. 3A, we obtained stiffening ratios (γ) , which quantify the differences in mechanical stiffness when jammed versus unjammed. First, we extracted the tangent modulus of elasticity [27]: $E_B = L^3 m/4bd^3$, where L is the support span, b is the width of the beam tested (mm), d is the depth of the beam tested (mm), and m is the slope of the tangent to the initial straight-line portion of the loaddeflection curve (N/mm). We then defined the stiffening ratio as: $\gamma = E_{Bi}/E_{Bu}$, where E_{Bi} and E_{Bu} are the jammed and unjammed effective bending moduli, respectively. Tangent moduli E_B were averaged across the five trials, and γ was calculated for each sample. The reported stiffening ratio is the average of the stiffening ratios of the three samples. The skins attained approximate stiffening ratios of $\gamma = 13.0$ when the loading anvil was loaded parallel to the actuators (similar to the results reported our prior work on jamming skins in [18]). When the anvil was oriented perpendicular to the actuators, they resisted bending, lowering the jamming ratio to $\gamma = 4.1$.

We note that the stiffening ratio γ was substantially less than that predicted by commonly used Coulombic layer jamming theory [15], [18], [16]. Theory predicts the stiffening ratio is equal to number of layers squared ($\gamma=N^2$, so $\gamma=250$ for our modules). We suspect that the discrepancy between experiment and theory derives from our assumption that the PET sheets are uniform sheets. In our experiments, the serpentine PET springs (introduced when we patterned the PET sheets to enable stretchability [18]) would occasionally buckle out-of-plane during bending, likely causing lower inter-layer friction and a smaller second moment of area (I), relative to a system of homogeneous sheets.

The PET VSRS can change their stiffness to lock into structures of various shapes and to suspend payloads (Fig. 3B). While the skins were designed primarily for dynamic robotic applications, they could also serve as standalone structures. For example, the skins can jam in an $\bf L$ shape or $\bf S$ shape as shown here, representing end-use cases including protecting scientific instruments and supporting payloads. Finally, we note that the minimum radius of curvature attained here was approximately 3 cm. Multiple lines of reasoning informed by our experiments with various VSRS designs suggest that smaller radii of curvature could be attained by using fewer jamming layers (since the lower bound of curvature for bent multi-layer systems of thickness h scales with 3/2h [17]), at the expense of lower payload-supporting capacity (since the jammed stiffness scales with h^3 [15], [18], [16]).

C. Locomotion

By using the actuators to generate motion, the sensors to detect motion, and the layer-jamming material of some of the modules to toggle stiffness, VSRSs can locomote in a variety of configurations and deliver payloads (Fig. 4 and Supplementary Videos 1 and 2). Here, we characterize the locomotion capabilities of our VSRSs in several configurations, ranging from single skins to several connected skins to achieve varied shapes.

First, to characterize the robot's arching motion independently of actual forward motion, we set a single VSRS on a

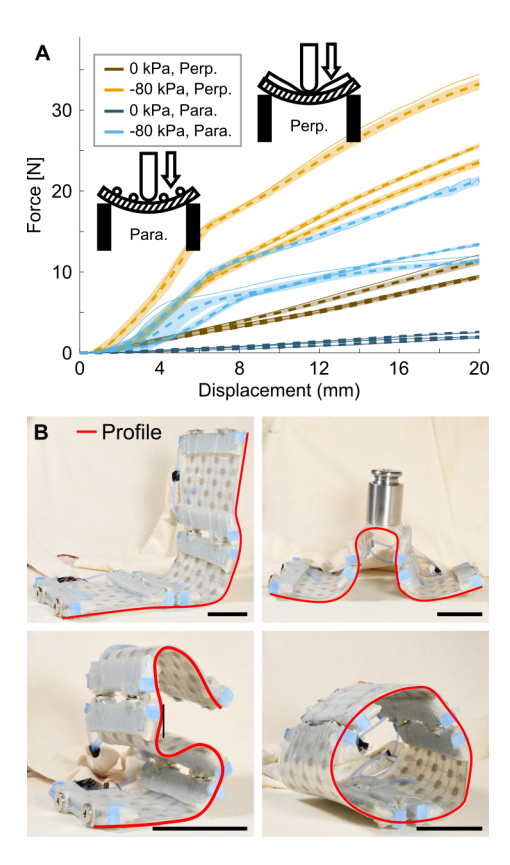


Fig. 3. PET VSRS can be mechanically stiffened upon application of vacuum pressure. (A) Mechanical characterization of PET VSRS in a three-point bending loading condition. The solid lines denote a single trial, while the dashed lines denote an average of five trials for a single sample, and the clouds represent ± 1 SD. "Perp." means the testing anvil was loaded perpendicular to the actuators, while "para." means the anvil was loaded parallel to the actuators. (B) A trio of VSRSs leveraging their variable-stiffness capabilities to create both open and closed structures. Left to right: Three modules jammed in an L shape as a standalone structure. A load-bearing Ω shape capable of holding a 1 kg weight. An "S" shape with curvatures concave in both directions. A closed cylindrical shape. Scale bars, 5 cm.

slippery acrylic plate and inflated it to 120 kPa over 25 seconds for 11 cycles. As the robot arched during inflation, the height of the midplane of the center of the VSRS was estimated by extracting the location of a red marker placed on the side of the robot using video (processed using MATLAB's Image Processing Toolbox). The results suggest an approximately quadratic relationship between height and pressure (Fig. 4A), while the small surface strains experienced by the stretch sensors resulted in the change in capacitance ΔC being roughly linear as a function of height h (Fig. 4B). Using the empirical relation for our PET VSRS determined from Fig. 4B (C = 42.95 - 0.20 * h), we then commanded the robot to to achieve a series of maximum arched heights using a bang-bang controller (Fig. 4C). After receiving a commanded maximum arch height, the robot would inflate its actuators until it reached the height, at which point the robot was immediately commanded to deflate. The robot was able to achieve multiple controlled arching sequences, which gave us confidence that the approach could be used to vary the arch height during locomotion.

Next, we used this closed-loop control to demonstrate

gait-based obstacle avoidance (Fig. 4D and Supplementary Video 1). In many real-world environments, obstacles and everyday objects will create overhangs that are smaller than the robot's typical arching height. Here, we simulated this with an overhang made of acrylic. The friction-biased acrylic feet allowed the robot to grip the ground and move across the surface by repeatedly arching and flattening. The robot could locomote with a fully arched motion up to an impasse (Fig. 4D(1-2)), then the set point was lowered so the robot could execute a flatter gait and pass below the overhang (Fig. 4D(3)). After clearing the obstacle, the robot could resume its faster, highly arched locomotion gait (Fig. 4D(4)).

Similar locomotion gaits can be attained in configurations with multiple modules connected in various topologies (Fig. 4E-G and Supplementary Video 2). While unimpeded by obstacles, a single module achieved an average speed of 2.70 BL/min. When carrying the 200 g payload in Fig. 4E, the robot was able to move at 0.78 BL/min. When at its destination, unjamming the top module allowed the robot to deploy its payload. Next, we attached three modules together serially and jammed the middle module upward to hold a weight (200 g) while the outer modules inflated their actuators to allow the trio to locomote (0.55 BL/min; Fig. 4F). When the middle module was unjammed, it could then assist the group to locomote (1.65 BL/min; Fig. 4G). Thus, by building equivalent functionality into each skin-variable stiffness capabilities, actuators, and sensors—each skin could be repurposed in situ to improve the functionality of the overall robot.

IV. MESH VSRS RESULTS

To illustrate how the VSRS concept can be realized with different components and component layouts, we instantiated a second VSRS design made with McKibben actuators and woven mesh jamming layers. Our primary objective during this design phase was to redesign the VSRS to be sufficiently deformable to serve as a continuum manipulator (where the "PET VSRS" design was empirically found to be too stiff for this function). We thus demonstrate the "mesh VSRS" modules achieving two canonical robotic tasks: locomotion and manipulation. For completeness, we also expanded the characterization of the mesh VSRS to include three-point bending and axial compression, with the skins wrapped in a cylindrical shape.

A. Manufacturing

To fabricate the mesh skins, we used a layer-by-layer method similar to that of the PET skins (Fig. 2). The sensor manufacturing process was nearly identical; however, to enable layer jamming, we added 50 layers of stretchable polyester tulle fabric mesh (Craft Forge) instead of PET. We then sewed on McKibben actuators made from latex balloons (Qualatex 260Q) that were inserted into polyester mesh sleeving (McMaster-Carr) and sealed with cable ties (McMaster-Carr). To keep the outer membrane and jamming layers in contact, we stitched through two points in the center and re-sealed the holes using EcoFlex 30. Finally, we used SilPoxy to attach velcro, add laser-cut acrylic feet, and improve the bond between the actuators and the membrane.

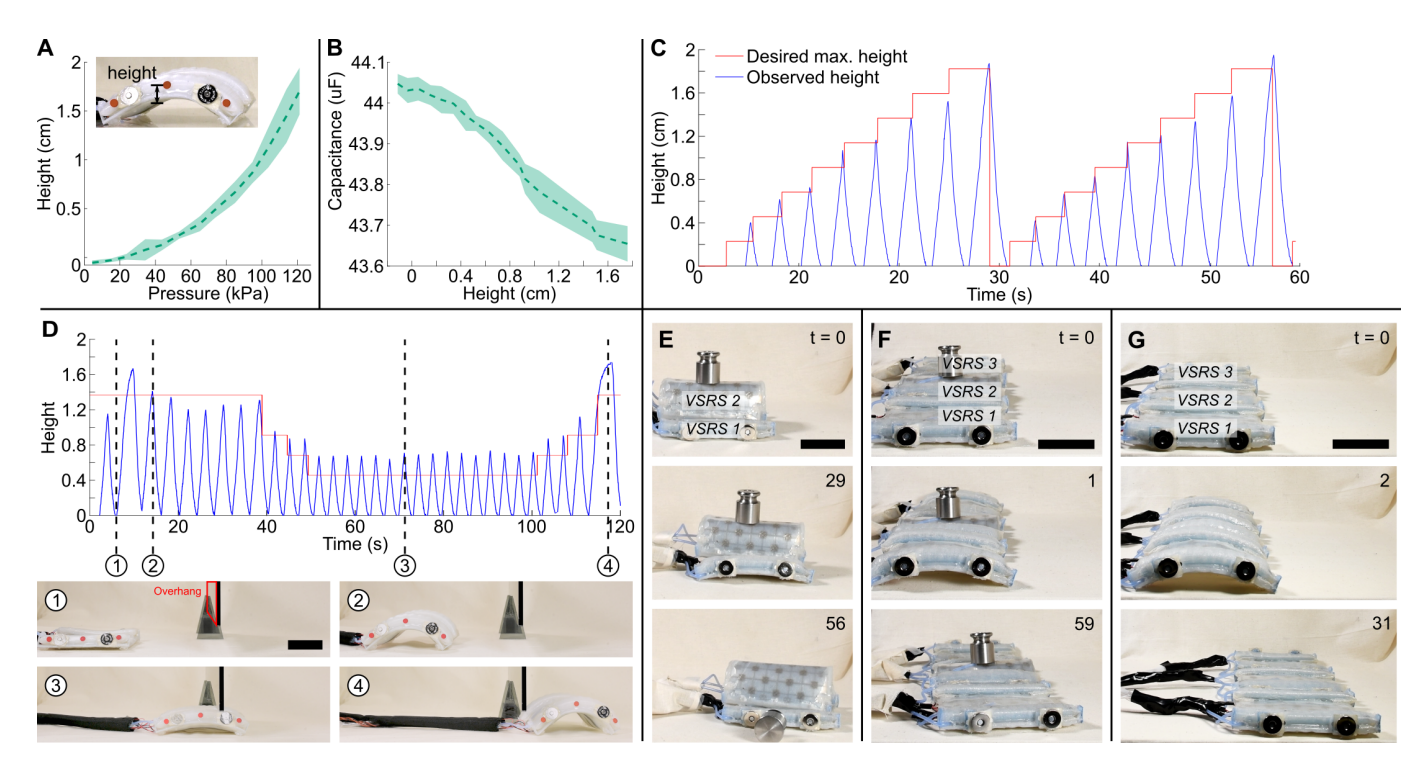


Fig. 4. Locomotion of PET VSRS, both solo (A-D) and connected in various topologies (E-G). (A) By inflating their PneuFlex actuators, the skins can arch upward, raising the center of their body relative to its initial starting height. (B) Sensor capacitance decreases as the robot curls, resulting in a roughly linear relationship between capacitance and height achieved. Dashed lines denote the mean over 11 cycles, while clouds depict ±1 standard deviation. (C) Executing a series of stepwise-increasing arched motions up to a desired maximum arch height, while the VSRS was stationary. After reaching the target height, the robot automatically deflated its actuators to return to a resting state. (D) A VSRS approaches an overhang and then executes a flatter gait to pass below the overhang, followed by additional highly-arched locomotion. Top: sensor data. Bottom: screenshots of actual VSRS motion, corresponding to the times marked in the top plot. The planar, rectangular overhang was reflective and has been highlighted with a red border in D1 for clarity. (E) One module locomoting with another payload-carrying module on top. When the top module unjammed, the weight was released into the environment. (F) Three modules connected in series, with the outer two serving as locomotors and the middle one jammed upward to hold a weight. (G) The middle module was then unjammed and used to aid in locomotion. Scale bars in (D-G) denote 5 cm.

B. Mechanical Characterization

To quantify the jamming behavior of the mesh VSRS, we conducted mechanical tests while the VSRSs were unjammed (at atmospheric pressure) and while jammed (at -80 kPa). We characterized the mesh VSRS in two three-point bending conditions while the skins were flat (with the test anvil loaded both parallel and perpendicular to the actuators, to match the PET VSRS characterization), and also added three-point bending and axial compression characterizations of the skins in a cylindrical configuration, since individual mesh skins could attain a cylindrical shape.

In the first three-point bending orientation, the actuators were aligned parallel to the loading anvil (with the supporting anvils spaced 80 mm apart), resulting in a stiffening ratio between jammed and unjammed states of $\gamma\approx 8.6:1.$ In the second orientation, the module was rotated 90 degrees so that the anvil load was applied to the actuators. The actuators resisted bending, raising the unjammed stiffness and lowering the stiffening ratio to $\gamma\approx 2.0:1.$ As a control study, we also tested three membranes that did not have sensors or actuators (under both loading conditions, at five repetitions each), finding that the stiffness ratio was $\gamma\approx 6.5:1$ when the loading anvil was aligned parallel to where the actuators would be aligned, and $\gamma\approx 2.4:1$ when rotated to be perpendicular. We suspect that this asymmetric bending stiffness is partially

due to the mesh's anisotropy. In this study, asymmetry allowed the VSRSs to achieve tighter curvatures, but in situations where isotropic behavior is desired, the mesh orientation could be alternated between successive layers.

To quantify the stiffness-changing capabilities of individual mesh skins in a cylindrical configuration, we first used a three-point bending setup (Fig. 5B). In this test, the same sample was tested five times. The loading anvil was lowered at a constant rate of 60 mm/min to a final displacement of 30 mm (with the supporting anvils spaced 80 mm apart). We observed that the module is roughly five times as rigid while cylindrical compared to the flat configuration, at both pressures, resulting in a moderate stiffening ratio of $\gamma \approx 3.0$. The higher stiffness can be attributed primarily to the greater moment of area while in the cylindrical shape (rigidity K = EI, where E is the effective modulus and I is the second moment of area).

Finally, three specimens were tested five times each in axial compression, with the modules curled in a cylindrical shape (Fig. 5C). The cylinder was 15 cm in height and approximately 5.5 cm in diameter, and the same loading rate was used as above (60 mm/min). To attain consistent vertical alignment, a polylactic acid (PLA) 3D-printed cylindrical base was attached to an acrylic plate. The base was inserted into the bottom of the curled specimen just deep enough that the base lined up with the active portion of the jamming membrane (i.e., to the edge

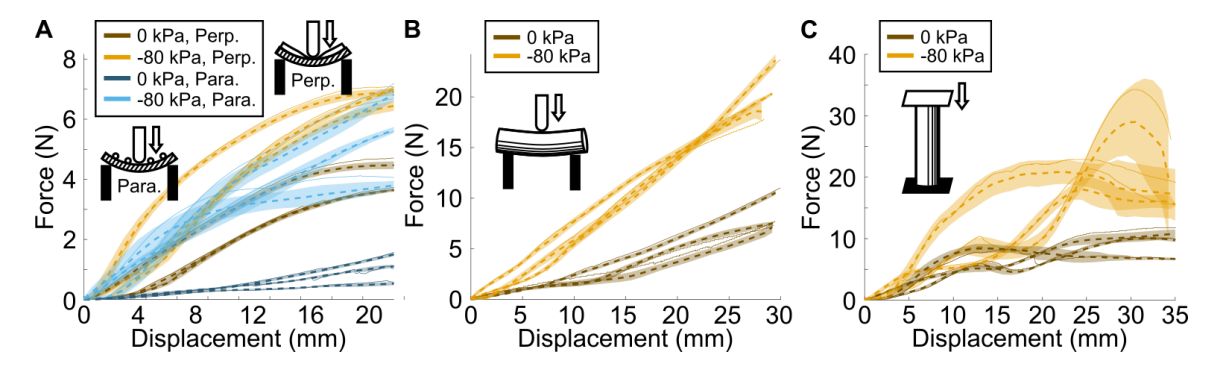


Fig. 5. Mesh VSRS were mechanically tested in three loading conditions. (A) Flat three-point bending, with the actuators pointing perpendicular ("perp.") to the loading anvil (as shown by the top illustration), versus parallel ("para.") to the loading anvil (as shown by the bottom illustration). (B) Three-point bending while in a cylindrical shape. (C) Axial compression while in a cylindrical shape. Note that the initial compression up to about 20 mm primarily corresponds to compressing the silicone borders, while compression and buckling of the jamming fabric primarily happens after 20 mm. In all plots (A-C), the dashed curves represent the mean over five trials of a single sample, while the solid curves denote a single representative load-displacement curve, and the clouds represent ± 1 SD.

of the silicone border). Two local force maxima were observed during many trials: the first corresponding to the buckling of the unsupported silicone edge on the top of the module, and the second corresponding to the buckling of the main, jamming portion of the module.

To evaluate the effect of jamming, we used the buckling ratio (BR): $BR = F_j/F_u$, where F_j is the force just before buckling of the jammed module (at the second peak), and F_u is the unjammed force at the same location. The five jammed and five unjammed force values were averaged separately for each sample, and then the buckling ratio was calculated for each sample. The average buckling ratio across three skins was ≈ 2.4 , similar to the ratios obtained in the other two loading conditions where the actuators bent (flat with anvil rotated 90 degrees, and cylindrical bending). This similarity supports what is predicted by taking the ratio of the Euler buckling load ($Fb = n\pi^2 EI/L^2$) while jammed and unjammed—most terms drop out, leaving us with the observation that BR should equal the ratio of the effective modulus, E_j/E_u .

C. Locomotion

By inflating their actuators to arch upward, Mesh VSRSs can locomote in a variety of configurations and deliver payloads (Fig. 6 and Video S3), similarly to the PET VSRSs. The friction-biased feet allow the skins to locomote, and the sensor data is captured in the same way. Moving over taut cotton muslin fabric, the single module was able to locomote at 2.80 BL/min; two connected modules moved the fastest, at 4.82 BL/min; while three modules connected together moved at 3.81 BL/min. Additionally, in the two-module configuration, each module could switch between contributing locomotive capabilities and holding a payload via jamming (Fig. 6C and Video S3). That is, one module locomotes used the inchworm gait, while the other gripped and held a payload, moving with the payload at 2.42 BL/min. When the robot reached its destination, the gripping module un-jammed to deliver its payload (Fig. 6C). The different surface strains experienced by all modules were captured in the sensory feedback for each shape-gait pair as shown in the graphs next to each set of photos in Fig. 6A-C.

D. Continuum Manipulator

With the more flexible jamming mesh, mesh VSRSs can be connected in series and curled into cylinders to create a continuum manipulator (Fig. 7 and Video S4). The lower module allowed the robot arm to lock into a given macro orientation, while the upper two modules used their actuators to reposition the arm in further smaller-scale manipulation actions.

A single module can be wrapped in a cylindrical shape to make a segment that can reposition its tip (Fig. 7A-C). We secured a module to a cylindrical foam base, with ≈ 3.5 cm overlap. The foam was affixed to a piece of acrylic with four motion-capture markers (for a PhaseSpace Improv motion-capture system) that defined a fixed local coordinate frame. A (fifth) motion-capture marker was placed on the top edge of the skin, to define the end-effector location. Then, we inflated the actuators one-by-one in sequence, with overlap, to move the segment around the perimeter of its attainable workspace. Projecting the workspace onto the XY plane, we see that the workspace is roughly a quadrilateral, with the corners attained when two neighboring actuators were fully inflated to 100 kPa (Fig. 7B).

For a given configuration, the sensor feedback tends to be repeatable throughout the motion space (Fig. 7C). The sensor with the highest observed capacitance change (sensor 3), for example, consistently increased its capacitance the most when actuators two and three were both inflated, while reading almost no change (unstretched) when those actuators were deflated. The other sensors showed unintuitive but repeatable trends, suggesting that *in situ* calibration would be desirable if precise motion within a workspace was necessary.

To demonstrate the capabilities unlocked through connecting multiple VSRS together in a multisegment manipulator configuration, we wrapped three VSRSs sequentially around a deformable cylinder to form a three-segment continuum arm. We then attached a motion-capture marker to the top VSRS. At the start of each trial, the bottom VSRS was manually reshaped and jammed to hold a new position. Then, the system inflated the actuators of the top two (unjammed) skins column-by-column (i.e., actuator 1 of both skins, followed by actuator

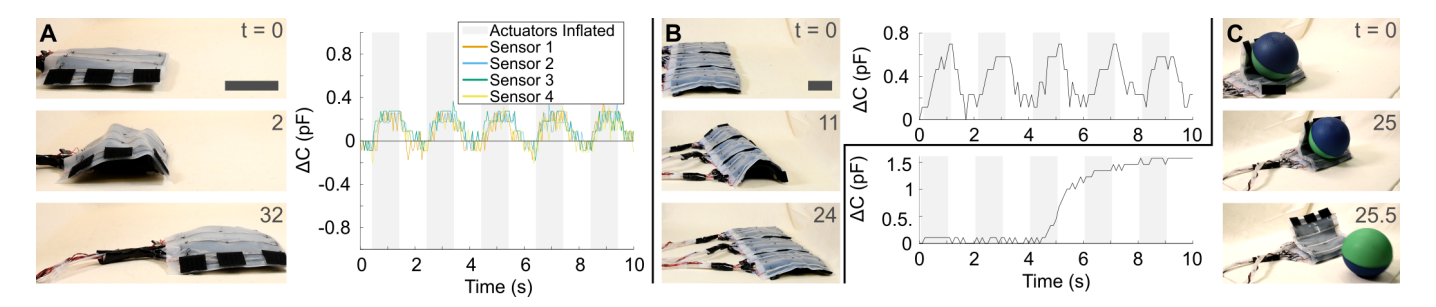


Fig. 6. Mesh VSRS can be reconfigured to adjust their functions. (A) A single VSRS executes an inchworm locomotion gait. Right: sensor feedback for all four sensors during five actuation cycles (a subset of the full locomotion sequence). (B) Three modules linked together can locomote in the same fashion. One sensor is plotted for clarity. (C) Two modules work together, one locomoting with an inchworm gait and one jammed on top to grip a payload. One sensor from the gripping module is plotted for clarity. The payload-carrying module can be un-jammed to deliver the payload. In (A,B), the scale bars denote 5 cm. In (C), an isometric view, the modules are identical to the other photos, with an edge length of 14 cm.

2 of both skins, etc.). A similar and approximately square motion path was attained for each trial, resulting in a series of overlapping local workspaces within the overall reach of the manipulator (Fig. 7E). The actuated skins reported repeatable sensor feedback across the trials, even though the bottom skin was jammed in a variety of dissimilar shapes (Fig. 7F).

V. CONCLUSION

In this manuscript, we introduced the concept of a variable stiffness robotic skin (VSRS): a reconfigurable robotic platform incorporating sensing, actuation, and variable stiffness materials in a skin-like form. We showed how VSRSs can be connected in different configurations to achieve tasks in locomotion and manipulation, while selectively stiffening to improve their individual or collective functionality in the absence of a host body. The actuators allowed the skins to move, while the sensors enabled closed-loop control, and the variable stiffness capabilities allowed the skins to be re-shaped in a given connection pattern, allowing another level of dynamic task adaptability. Finally, we showed two embodiments that highlight the richness of the design space, allowing mission constraints to be accommodated by selecting appropriate actuators, sensors, and materials. In our particular embodiments—PET VSRS and mesh VSRS—the mesh VSRS design traded a decreased maximum stiffness for increased deformability, enabling it to better serve in a continuum manipulation context.

In future work, we plan to improve the shape-sensing capabilities of VSRS by calibrating a data-driven shape estimation algorithm, such as that proposed by Truby et al. [28], for each new VSRS topology. Thin bending actuators, such as SMA ribbons [29], could then be integrated to enable a VSRS to autonomously achieve even more complex shapes. Additionally, the trade-off between payload-carrying capacity and moldability could be overcome by utilizing variableelasticity materials to enhance the unjammed stretchability and the jammed stiffness [30]. Finally, we note that for full proprioception, it would be useful to integrate vacuum sensors into the VSRS to verify proper jamming was achieved. Paired with advances in other areas—including actuation, sensing, variable stiffness materials, and control-VSRSs could serve additional applications, such as adaptable linkages in larger robots, smart reconfigurable garments, and reconfigurable active structures.

REFERENCES

- D. J. Blackiston, T. Shomrat, and M. Levin, "The stability of memories during brain remodeling: A perspective," *Communicative & Integrative Biology*, vol. 8, p. e1073424, Oct. 2015.
- [2] Y. Yekutieli, R. Sagiv-Zohar, R. Aharonov, Y. Engel, B. Hochner, and T. Flash, "Dynamic Model of the Octopus Arm. I. Biomechanics of the Octopus Reaching Movement," *Journal of Neurophysiology*, vol. 94, pp. 1443–1458, Aug. 2005. Publisher: American Physiological Society.
- [3] D. Shah, B. Yang, S. Kriegman, M. Levin, J. Bongard, and R. Kramer-Bottiglio, "Shape Changing Robots: Bioinspiration, Simulation, and Physical Realization," *Advanced Materials*, vol. n/a, no. n/a, p. 2002882, 2020.
- [4] D. S. Shah, J. P. Powers, L. G. Tilton, S. Kriegman, J. Bongard, and R. Kramer-Bottiglio, "A soft robot that adapts to environments through shape change," *Nature Machine Intelligence*, vol. 3, no. 1, pp. 51–59, 2021.
- [5] R. Baines, S. K. Patiballa, J. Booth, L. Ramirez, T. Sipple, A. Garcia, F. Fish, and R. Kramer-Bottiglio, "Multi-environment robotic transitions through adaptive morphogenesis," *Nature*, vol. 610, no. 7931, pp. 283– 289, 2022.
- [6] M. Manti, V. Cacucciolo, and M. Cianchetti, "Stiffening in Soft Robotics: A Review of the State of the Art," *IEEE Robotics Automation Magazine*, vol. 23, pp. 93–106, Sept. 2016.
- [7] M. Yim, W. m. Shen, B. Salemi, D. Rus, M. Moll, H. Lipson, E. Klavins, and G. S. Chirikjian, "Modular Self-Reconfigurable Robot Systems [Grand Challenges of Robotics]," *IEEE Robotics Automation Magazine*, vol. 14, pp. 43–52, Mar. 2007.
- [8] M. A. Robertson and J. Paik, "New soft robots really suck: Vacuum-powered systems empower diverse capabilities," Science Robotics, vol. 2, Aug. 2017. Publisher: Science Robotics Section: Research Article.
- [9] S. Li, S. A. Awale, K. E. Bacher, T. J. Buchner, C. D. Santina, R. J. Wood, and D. Rus, "Scaling Up Soft Robotics: A Meter-Scale, Modular, and Reconfigurable Soft Robotic System," *Soft Robotics*, Apr. 2022. Publisher: Mary Ann Liebert, Inc., publishers 140 Huguenot Street, 3rd Floor New Rochelle, NY 10801 USA.
- [10] J. W. Booth, D. Shah, J. C. Case, E. L. White, M. C. Yuen, O. Cyr-Choiniere, and R. Kramer-Bottiglio, "OmniSkins: Robotic skins that turn inanimate objects into multifunctional robots," *Science Robotics*, vol. 3, p. eaat1853, Sept. 2018.
- [11] J. C. Case, M. C. Yuen, J. Jacobs, and R. Kramer-Bottiglio, "Robotic Skins That Learn to Control Passive Structures," *IEEE Robotics and Automation Letters*, vol. 4, pp. 2485–2492, July 2019.
- [12] D. S. Shah, M. C. Yuen, L. G. Tilton, E. J. Yang, and R. Kramer-Bottiglio, "Morphing Robots Using Robotic Skins That Sculpt Clay," *IEEE Robotics and Automation Letters*, vol. 4, pp. 2204–2211, Apr. 2019.
- [13] M. C. Yuen, R. A. Bilodeau, and R. K. Kramer, "Active Variable Stiffness Fibers for Multifunctional Robotic Fabrics," *IEEE Robotics* and Automation Letters, vol. 1, pp. 708–715, July 2016.
- [14] K. Suzumori, S. Wakimoto, K. Miyoshi, and K. Iwata, "Long bending rubber mechanism combined contracting and extending fluidic actuators," in 2013 IEEE/RSJ International Conference on Intelligent Robots and Systems, pp. 4454–4459, Nov. 2013. ISSN: 2153-0866.

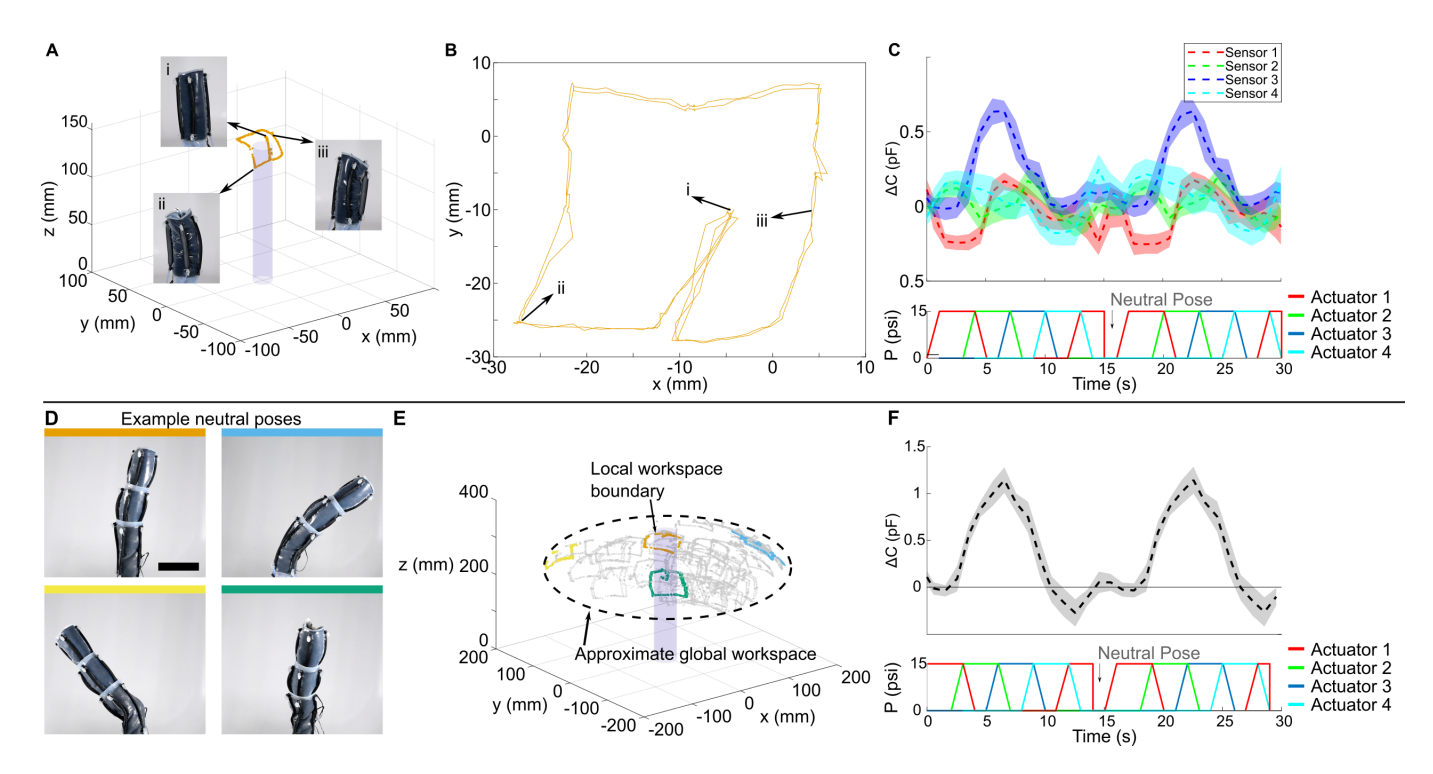


Fig. 7. Mesh VSRS connected to form a continuum manipulator. (A) A single curled skin can reposition its end-effector in 3D. Insets show the manipulator in three states: i, neutral; ii, bending using two actuators; iii, bending using one actuator. (B) When projected into the XY plane, the workspace boundary is approximately a quadrilateral. For clarity, two actuation cycles are plotted. (C) Sensor feedback during motion. Dashed lines denote the mean, while error clouds denote ± 1 standard deviation, across 16 trials. (D-F) Multiple skins connected in series can serve as a multi-segment manipulator. (D) A subset of the modules can be jammed in different poses, allowing the remaining modules to actuate the manipulator for more precise local 3D motions. Scale bar, 5 cm. (E) The resulting 3D workspaces for each pose in (D), along with other example poses (shown in gray), are combined in a single plot. (F) Sensory feedback for the dominant sensor from the middle (most bent) module, corresponds to local motions about these jammed poses. Dashed lines denote the mean, while error clouds denote ± 1 standard deviation, across 76 trials.

- [15] Narang Yashraj S., Vlassak Joost J., and Howe Robert D., "Mechanically Versatile Soft Machines through Laminar Jamming," Advanced Functional Materials, vol. 0, p. 1707136, Feb. 2018.
- [16] S. Kawamura, T. Yamamoto, D. Ishida, T. Ogata, Y. Nakayama, O. Tabata, and S. Sugiyama, "Development of passive elements with variable mechanical impedance for wearable robots," in *Proceedings* 2002 IEEE International Conference on Robotics and Automation (Cat. No.02CH37292), vol. 1, pp. 248–253 vol.1, 2002.
- [17] W. M. v. Rees, E. Vouga, and L. Mahadevan, "Growth patterns for shape-shifting elastic bilayers," *Proceedings of the National Academy* of Sciences, p. 201709025, Oct. 2017.
- [18] D. S. Shah, E. J. Yang, M. C. Yuen, E. C. Huang, and R. Kramer-Bottiglio, "Jamming Skins that Control System Rigidity from the Surface," *Advanced Functional Materials*, vol. 31, no. 1, p. 2006915, 2021.
- [19] T. Mitsuda, "Variable-stiffness Sheets Obtained using Fabric Jamming and their applications in force displays," in 2017 IEEE World Haptics Conference (WHC), pp. 364–369, June 2017.
- [20] N. El-Atab, R. B. Mishra, F. Al-Modaf, L. Joharji, A. A. Alsharif, H. Alamoudi, M. Diaz, N. Qaiser, and M. M. Hussain, "Soft Actuators for Soft Robotic Applications: A Review," *Advanced Intelligent Systems*, vol. 2, no. 10, p. 2000128, 2020.
- [21] D. Chen and Q. Pei, "Electronic Muscles and Skins: A Review of Soft Sensors and Actuators," *Chemical Reviews*, vol. 117, pp. 11239–11268, Sept. 2017.
- [22] R. Deimel and O. Brock, "A compliant hand based on a novel pneumatic actuator," in 2013 IEEE International Conference on Robotics and Automation, pp. 2047–2053, May 2013.
- [23] X. Wang, L. Fan, J. Zhang, X. Sun, H. Chang, B. Yuan, R. Guo, M. Duan, and J. Liu, "Printed Conformable Liquid Metal e-Skin-Enabled Spatiotemporally Controlled Bioelectromagnetics for Wireless Multisite Tumor Therapy," Advanced Functional Materials, vol. 29, no. 51, p. 1907063, 2019.
- [24] C.-P. Chou and B. Hannaford, "Measurement and modeling of McKibben pneumatic artificial muscles," *IEEE Transactions on Robotics and Automation*, vol. 12, pp. 90–102, Feb. 1996.

- [25] S. Y. Kim, R. Baines, J. Booth, N. Vasios, K. Bertoldi, and R. Kramer-Bottiglio, "Reconfigurable soft body trajectories using unidirectionally stretchable composite laminae," *Nature Communications*, vol. 10, p. 3464, Aug. 2019.
- [26] J. W. Booth, J. C. Case, E. L. White, D. S. Shah, and R. Kramer-Bottiglio, "An addressable pneumatic regulator for distributed control of soft robots," in 2018 IEEE International Conference on Soft Robotics (RoboSoft), pp. 25–30, Apr. 2018.
- [27] D20 Committee, "ASTM D790: Test Methods for Flexural Properties of Unreinforced and Reinforced Plastics and Electrical Insulating Materials," tech. rep., ASTM International, 2010.
- [28] R. L. Truby, C. D. Santina, and D. Rus, "Distributed Proprioception of 3D Configuration in Soft, Sensorized Robots via Deep Learning," *IEEE Robotics and Automation Letters*, vol. 5, pp. 3299–3306, Apr. 2020. Conference Name: IEEE Robotics and Automation Letters.
- [29] T. L. Buckner, R. A. Bilodeau, S. Y. Kim, and R. Kramer-Bottiglio, "Roboticizing fabric by integrating functional fibers," *Proceedings of the National Academy of Sciences*, Sept. 2020. Publisher: National Academy of Sciences Section: Physical Sciences.
- [30] T. L. Buckner, M. C. Yuen, S. Y. Kim, and R. Kramer-Bottiglio, "Enhanced Variable Stiffness and Variable Stretchability Enabled by Phase-Changing Particulate Additives," *Advanced Functional Materials*, vol. 29, no. 50, p. 1903368, 2019.